JACS
JOURNAL OF THE AMERICAN CHEMICAL SOCIETY

Communication

pubs.acs.org/JACS

Photocurrent Enhancement from Diketopyrrolopyrrole Polymer Solar Cells through Alkyl-Chain Branching Point Manipulation

Iain Meager,*[,†] Raja Shahid Ashraf,[†] Sonya Mollinger,[§] Bob C. Schroeder,[†] Hugo Bronstein,[∥] Daniel Beatrup,[†] Michelle S. Vezie,[‡] Thomas Kirchartz,[‡] Alberto Salleo,[§] Jenny Nelson,[‡] and Iain McCulloch[†]

[†]Department of Chemistry and Centre for Plastic Electronics, Imperial College London, London SW7 2AZ, U.K.
[‡]Department of Physics and Centre for Plastic Electronics, Imperial College London, London SW7 2AZ, U.K.
[§]Department of Materials Science and Engineering, Stanford University, Stanford, California 94305, United States
[∥]Department of Chemistry, University College London, London WC1H 0AJT, U.K.

Supporting Information

ABSTRACT: Systematically moving the alkyl-chain branching position away from the polymer backbone afforded two new thieno[3,2-*b*]thiophene−diketopyrrolopyrrole (DPPTT-T) polymers. When used as donor materials in polymer:fullerene solar cells, efficiencies exceeding 7% were achieved without the use of processing additives. The effect of the position of the alkyl-chain branching point on the thin-film morphology was investigated using X-ray scattering techniques and the effects on the photovoltaic and charge-transport properties were also studied. For both solar cell and transistor devices, moving the branching point further from the backbone was beneficial. This is the first time that this effect has been shown to improve solar cell performance. Strong evidence is presented for changes in microstructure across the series, which is most likely the cause for the photocurrent enhancement.

The desirable optical and electrical properties exhibited by conjugated semiconducting polymers make them promising candidate materials for use in the next generation of solar cells and organic field-effect transistors (OFETs). Their solution processability provides the potential for large-scale inexpensive manufacture, and their lightweight and flexible nature leads to a large number of potential applications currently beyond the scope of conventional inorganic cells. To date, one of the most promising classes of polymer materials are diketopyrrolopyrrole (DPP)-based polymers, which have shown some of the highest solar cell efficiencies reported to date and have been used to fabricate transistor devices with good ambipolarity and mobilities that routinely surpass 1 $cm^2\ V^{-1}\ s^{-1}$.[1−6] The DPP unit has an electron-withdrawing core, which is typically flanked by an electron-rich unit. Copolymerization with an electron-rich comonomer can afford a range of extended push−pull-type conjugated polymers. The backbone planarity promotes strong interchain $\pi-\pi$ interactions that in turn can facilitate good charge transport. In the design of semiconducting polymers, a large amount of effort is focused on band-gap engineering via control over the backbone electron distribution. Thus, the effect of the solubilizing alkyl chains has been less studied, despite literature demonstrating their importance.[7−13] Differences between branched and linear alkyl chains and the resultant influence on the photovoltaic performance have been demonstrated.[14−17] Further studies have found that the specific effect of the alkyl-chain branching position can be critical, with related work on transistor devices showing improved charge carrier mobilities.[18,19] However, the effect of this on solar cell performance has yet to be examined. We previously demonstrated the promising performance of DPPTT-T in solar cell and OFET devices. The effect of the side-chain branching point on the performance and processability of solar cells made with this polymer is therefore of interest.[20] By moving the branching point from its regular position relatively close to the polymer backbone, as in the original DPPTT-T polymer (**C1**), to positions further from the backbone, we aimed to determine whether the $\pi-\pi$ stacking distance could be influenced and to evaluate the effect that this would have on the crystallinity, morphology, and photovoltaic properties.

The three DPPTT-T polymers **C1**, **C2**, and **C3** (Figure 1), where **C*n*** refers to the number of linear carbon atoms between the alkylated nitrogen and the alkyl-chain branching point, were synthesized by copolymerization of their respective monomeric units with thiophene. The monomers were synthesized by alkylation of the DPPTT core with the corresponding alkyl iodide. All of the alkyl chains were synthesized from

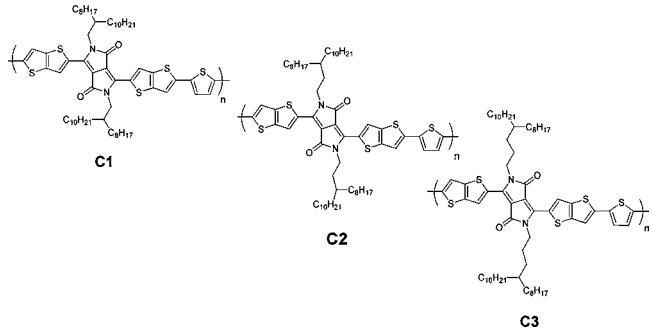

Figure 1. Chemical structures of **C1**−**C3**.

Received: July 8, 2013
Published: July 22, 2013

   dx.doi.org/10.1021/ja406934j | *J. Am. Chem. Soc.* 2013, 135, 11537−11540

Table 1. Properties of C1−C3

polymer	M_n (kDa)[a]	M_w (kDa)[a]	PDI[a]	λ_{max} (nm) film[b]	λ_{max} (nm) solution[c]	E_{HOMO} (eV) PESA[d]	E_{HOMO} (eV) CV[e]	E_{LUMO} (eV) PESA[d]	E_{LUMO} (eV) CV[e]	band gap (eV)[f]
C1	24	89	3.7	790	764	−5.1	−5.1	−3.7	−3.6	1.4
C2	45	83	1.8	810	812	−5.1	−5.1	−3.7	−3.4	1.4
C3	80	154	1.9	803	804	−5.1	−5.1	−3.7	−3.5	1.4

[a]Number-average and weight-average molecular weights (M_n and M_w, respectively) and weight-average polydispersity indexes (PDI = M_w/M_n) determined by gel-permeation chromatography using low-PDI (<1.10) polystyrene standards and chlorobenzene as the eluent. [b]Spin-coated from 5 mg/mL chlorobenzene solution. [c]Measured in dilute chlorobenzene solution. [d]HOMO energies (E_{HOMO}) measured by PESA and LUMO energies (E_{LUMO}) estimated by adding the UV−vis absorption onset to E_{HOMO}. [e]Measured by cyclic voltammetry [f]Estimated as the difference between the experimentally determined E_{HOMO} and the optically estimated E_{LUMO}.

commercially available 2-octyl-1-dodecanol. To move the branching position two carbons from the polymer backbone in **C2**, the alkyl chain was obtained by Grignard reaction of the corresponding alkyl bromide with paraformaldehyde followed by iodination to afford 3-octyl-1-tridecyl iodide. The alkyl chain with the branching point three carbons from the backbone in **C3** was synthesized by formation of the corresponding malonic ester from the alkyl bromide, hydrolysis to give the acid, and subsequent reduction to the alcohol followed by iodination to afford 4-octyl-1-tetradecyl iodide. **C1**−**C3** were synthesized under Pd-catalyzed Stille coupling conditions using microwave irradiation. Full synthetic details are included in the Supporting Information (SI). After polymerization, the polymers were precipitated into methanol and purified by Soxhlet extraction in acetone and hexane (24 h each) to remove catalytic impurities and lower-molecular-weight oligomers. The purified polymers were removed from the Soxhlet thimble with chloroform and finally chlorobenzene. Of the polymers, **C3** with the largest alkyl chain was the most soluble, allowing us to achieve a very high number-average molecular weight (M_n) of 80 kDa, whereas in the case of **C2** not all of the material could be solubilized in chlorobenzene, thus leading to a slightly lower M_n of 45 kDa. The solubility of **C3** was noticeably improved relative to that of the original polymer **C1**, with all of the polymeric material dissolving in chloroform. Both **C2** and **C3** had improved solubility relative to **C1**, which is reflected in their higher molecular weights and narrower polydispersities (Table 1).

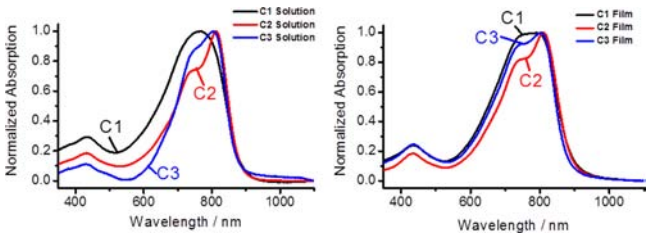

Figure 2. UV−vis absorption spectra of **C1**−**C3** in (left) chlorobenzene solution and (right) thin films spun from chlorobenzene.

UV−vis absorption spectra of **C1**−**C3** are shown in Figure 2. The absorption maxima of both **C2** and **C3** are red-shifted in solution and thin films relative to those of **C1**. **C2** and **C3** show narrow absorption profiles with observable shoulders at lower wavelengths, whereas the absorption band of **C1** shows a far less pronounced vibronic structure. Interestingly, both of the longer-alkyl-chain polymers show negligible red shifts in going from solution to the solid state, in contrast to **C1**, which shows a significant red shift of ∼30 nm. In the case of **C2** and **C3**, the alkyl-chain branching point is further away from the DPP core, which allows stronger intermolecular $\pi-\pi$ stacking of the aromatic rings, ultimately leading to enhanced molecular aggregation in solution and similar absorption features in solution and the solid state. For **C1**, however, the proximity of the alkyl-chain branching point to the DPP core possibly hinders the $\pi-\pi$ stacking and aggregation in solution; this is overcome by intermolecular forces in the solid state, planarizing the backbone and thus causing a significant red shift in the solid-state UV−vis absorption bands relative to the solution spectrum. The frontier molecular orbital energies (E_{HOMO} and E_{LUMO}) were determined using photoelectron spectroscopy in air (PESA) and the absorption onsets from the UV−vis spectra and were further investigated by cyclic voltammetry (Table 1); it appears that manipulating the alkyl-chain branching point has little effect on E_{HOMO} and E_{LUMO}.

Bulk heterojunction (BHJ) solar cells were fabricated using **C1**, **C2**, or **C3** as the donor material in the active layer by spin-coating of a 1:2 polymer/$PC_{71}BM$ mixture from a 4:1 chloroform:*o*-dichlorobenzene solvent mixture. Cells were prepared and tested under simulated 100 mW/cm AM1.5G illumination. Device fabrication details are given in the SI. The current density−voltage ($J-V$) curves averaged over the pixels of the best-performing substrate and representative external quantum efficiency (EQE) spectra are shown in Figure 3. The open-circuit voltage (V_{oc}), short-circuit current (J_{sc}), fill factor (FF), and power conversion efficiency (PCE) of the best performing pixel of each type are summarized in Table 2. Both

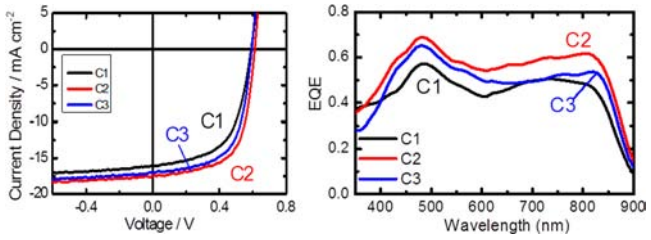

Figure 3. (left) $J-V$ curves for **C1**−**C3** averaged over the pixels on the best-performing substrates and (right) EQE spectra for typical blend devices using **C1**−**C3**.

Table 2. Solar Cell Device Characterstics of C1−C3 Taken from the Best-Performing Pixel of Each Type

polymer	J_{sc} (mA/cm^2)	V_{oc} (V)	FF	PCE (%)
C1	16.6	0.59	0.60	5.9
C2	18.6	0.61	0.64	7.3
C3	18.7	0.60	0.62	6.9

dx.doi.org/10.1021/ja406934j | J. Am. Chem. Soc. 2013, 135, 11537−11540

Table 3. OFET Properties of C1−C3 in Devices with a Bottom-Gate Top-Contact Architecture

polymer	$d_{\pi-\pi}$ (Å^{-1})[a]	μ_{hole} (cm^2 V^{-1} s^{-1})[b]	V_{th} (V)[c]	I_{on}/I_{off}[c]
C1	1.75	0.014	−20	∼5 × 10^2
C2	1.78	0.052	−17	∼1 × 10^3
C3	1.78	0.066	−15	∼1 × 10^3

[a]Polymer $\pi-\pi$ stacking distances as measured by 2D GIXS. [b]Highest effective hole mobilities measured in the saturation regime. [c]Threshold voltages (V_{th}) and on/off ratios (I_{on}/I_{off}) extracted from the linear regime (V_d = −5 V).

C2 and **C3** show V_{oc} values comparable to that of **C1**, which is in good agreement with the similar E_{HOMO} values measured by PESA and validates the idea that the improved photocurrent arising from increased branching point distance is not a result of changes in the polymer energy levels. The most dramatic improvement is seen in the J_{sc} of **C2** and **C3** (18.6 and 18.7 mA/cm^2 respectively). The very high J_{sc} values together with good FF and V_{oc} values resulted in PCEs of 7.3% for **C2** and 6.9% for **C3**, up from 5.9% for **C1**. The EQE spectra confirmed the higher photocurrent generation efficiencies for the devices made with **C2** and **C3** relative to **C1**. Bottom-gate top-contact OFETs with gold source and drain electrodes were fabricated to directly compare the trend in the hole transport properties of **C1**−**C3** (Table 3); further details and representative transfer and output curves are included in the SI. The recorded hole mobilities (μ_{hole}) were significantly improved, showing a trend similar to the improvements observed in the solar cell properties with increasing distance between the nitrogen and the branching position in **C2** and **C3**. It should be noted that the mobilities recorded for these polymers are noticeably lower than those previously published for **C1** devices. The initial testing for the present series of polymers was performed with a bottom-gate top-contact device architecture, whereas the previous high-performance transistor mobilities for **C1** were observed with a top-gate bottom-contact architecture. Although the μ_{hole} values are lower than those reported previously for **C1**, the promising trend in μ_{hole} with branching point position indicates that higher mobilities will be realized for polymers **C2** and **C3** in optimized FET device structures.

We used 2D grazing-incidence X-ray scattering (GIXS) to study films of the pure polymers (Figure 4) and 1:2 (w/w) **Cn**/PC[71]BM blend films (Figure 5). The component of the

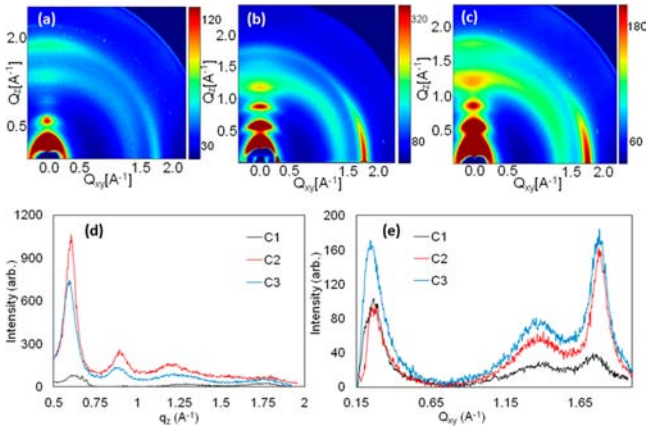

Figure 4. (a−c) 2D GIXS patterns of (a) **C1**, (b) **C2**, and (c) **C3** films. (d, e) Line cuts in the (d) q_z and (e) Q_{xy} directions.

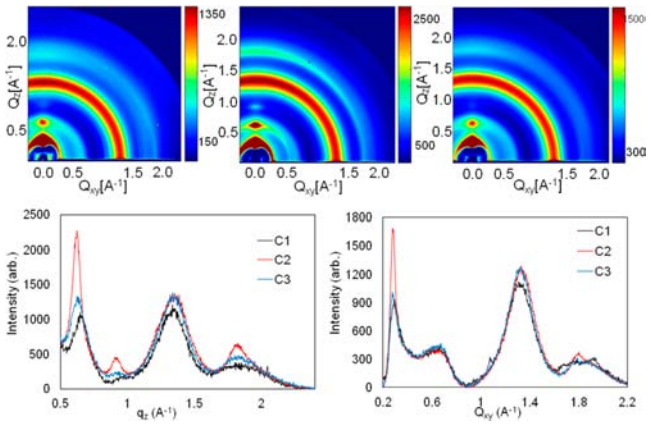

Figure 5. (a−c) 2D GIXS patterns of **Cn**/PC[71]BM blend films using (a) **C1**, (b) **C2**, and (c) **C3**. (d, e) Line cuts in the (d) q_z and (e) Q_{xy} directions.

scattering vector parallel to the substrate plane is given by Q_{xy}, and q_z is the component perpendicular to the substrate plane. In general, shifting the branching point away from the backbone seemed to increase the crystallinity of the cast films of **C2** and **C3** relative to **C1**. Furthermore, in the neat polymer films, the (200) peak shifts to slightly lower q with increasing branching point distance: for **C1**−**C3**, the (200) peak is located at q_z = 0.62, 0.60, and 0.59 Å^{-1}, respectively (Figure 4a−c; Figure 4d displays line cuts showing relative peak distances). The location of the π-stacking peak is also weakly dependent on the polymer and is located at 1.78 Å^{-1} for **C2** and **C3** and 1.75 Å^{-1} for **C1** (Figure 4e). However, the texture of the neat polymer film is strongly dependent on the location of the branching point. It is interesting to note that **C1** exhibits a pronounced face-on character, while both **C2** and **C3** have significant edge-on character. Thus, the more distant branching points in **C2** and **C3** seem to encourage an edge-on morphology in the neat polymer films. Similar variations have previously been noticed with DPP polymers, and more detailed studies of these differences are ongoing.[21] In the blend films (Figure 5), the GIXS patterns contain peaks associated with the pure polymers in addition to a diffraction halo peaked near 1.33 Å^{-1} associated with the PC[71]BM amorphous phase. The diffraction patterns of the blends also show a set of alkyl-stacking peaks, located at 0.65 Å^{-1} for **C1**, 0.62 Å^{-1} for **C2**, and 0.63 Å^{-1} for **C3** (Figure 5d). These are shifted slightly toward higher q from their positions in the pure films, indicating that in the blends the lamellar spacing is narrower than in the pure films. The blend films also show a diffraction feature located near 1.79 Å^{-1}, roughly the same location as the π-stacking peak found in the pure films. For **C2** (Figure 5b) the widths of this peak in the q_{xy} direction are similar [0.08 Å^{-1} for the neat film (Figure 4e) and 0.11 Å^{-1} for the blend (Figure 5e)]; for **C3** they are 0.14 Å^{-1} in the neat film and 0.16 Å^{-1} in the blend. Thus, the coherence length in the π-stacking direction is not reduced by blending. In the blend with **C2** in particular, the polymer assumes a nearly isotropic texture, which is more favorable for out-of-plane transport in solar cells. Analysis of the (200) lamellar peak intensities in the q_z direction for the polymer blend films with PC[71]BM shows a substantial increase in intensity upon going from the **C1** blend to the **C2** blend. Though a truly quantitative comparison cannot be made for different materials, this qualitative comparison of the intensities suggests that at a larger branching point distance, the crystallinity of the film increases in

dx.doi.org/10.1021/ja406934j | J. Am. Chem. Soc. 2013, 135, 11537−11540

the blends similarly to what was observed in the neat polymer films. The same trend is preserved for the π-stacking peak.

In summary, we have prepared two new DPPTT-T based copolymers by systematically moving the alkyl-chain branching point. These polymers exhibit high solar cell performance, giving efficiencies in excess of 7% without the use of processing additives. X-ray scattering analysis showed that the location of the branching point can influence the orientation of the conjugated backbone plane and that the improvement in solar cell and OFET performance upon moving the branching point further from the backbone is most likely a result of improved crystallinity of the polymer in the neat and blend films.

■ ASSOCIATED CONTENT

Supporting Information

Synthesis of monomers and copolymers, solar cell and OFET characteristics and fabrication, GIXD measurements, and cyclic voltamograms. This material is available free of charge via the Internet at http://pubs.acs.org.

■ AUTHOR INFORMATION

Corresponding Author

i.meager11@imperial.ac.uk

Notes

The authors declare no competing financial interest.

■ ACKNOWLEDGMENTS

This work was carried out primarily with funding and support from The Leventis Foundation, the National Research Fund of Luxembourg, and the X10D Project (EP 287818). H.B. and T.K. acknowledge support via Imperial College Junior Research Fellowships. M.S.V. and J.N. acknowledge support from the Engineering and Physical Sciences Research Council.

■ REFERENCES

(1) Nielsen, C. B.; Turbiez, M.; McCulloch, I. *Adv. Mater.* **2013**, *25*, 1859.
(2) Qu, S.; Tian, H. *Chem. Commun.* **2012**, *48*, 3039.
(3) Kronemeijer, A. J.; Gili, E.; Shahid, M.; Rivnay, J.; Salleo, A.; Heeney, M.; Sirringhaus, H. *Adv. Mater.* **2012**, *24*, 1558.
(4) Dou, L.; Gao, J.; Richard, E.; You, J.; Chen, C.-C.; Cha, K. C.; He, Y.; Li, G.; Yang, Y. *J. Am. Chem. Soc.* **2012**, *134*, 10071.
(5) Lee, J.; Han, A. R.; Kim, J.; Kim, Y.; Oh, J. H.; Yang, C. *J. Am. Chem. Soc.* **2012**, *134*, 20713.
(6) Kanimozhi, C.; Yaacobi-Gross, N.; Chou, K. W.; Amassian, A.; Anthopoulos, T. D.; Patil, S. *J. Am. Chem. Soc.* **2012**, *134*, 16532.
(7) Tsao, H. N.; Cho, D. M.; Park, I.; Hansen, M. R.; Mavrinkskiy, A.; Yoon, D. Y.; Graf, R.; Pisula, W.; Spiess, H. W.; Müllen, K. *J. Am. Chem. Soc.* **2011**, *133*, 2605.
(8) Kline, R. J.; Delongchamp, D. M.; Fischer, D. A.; Lin, E. K.; Richter, L. J.; Chabinyc, M.; Toney, M. F.; Heeney, M.; McCulloch, I. *Macromolecules* **2007**, *40*, 7960.
(9) Osaka, I.; Abe, T.; Shinamuru, S.; Miyazaki, E.; Takimiya, K. *J. Am. Chem. Soc.* **2010**, *132*, 5000.
(10) Savage, R. C.; Orgiu, E.; Mativetsky, J. M.; Pisula, W.; Schnitzler, T.; Eversloh, C. L.; Li, C.; Müllen, K.; Samori, P. *Nanoscale* **2012**, *4*, 2387.
(11) Cabanetos, C.; El Labban, A.; Bartelt, J. A.; Douglas, J. D.; Mateker, W. R.; Fréchet, J. M. J.; McGehee, M. D.; Beaujuge, P. M. *J. Am. Chem. Soc.* **2013**, *135*, 4656.
(12) Thompson, B. C.; Kim, B. J.; Kavulak, D. F.; Sivula, K.; Mauldin, C.; Fréchet, J. M. J. *Macromolecules* **2007**, *40*, 7425.
(13) Liang, Y.; Feng, D.; Wu, Y.; Tsai, S.-T.; Li, G.; Ray, C.; Yu, L. *J. Am. Chem. Soc.* **2009**, *131*, 7792.
(14) Bronstein, H.; Leem, D. S.; Hamilton, R.; Woebkenberg, P.; King, S.; Zhang, W.; Ashraf, R. S.; Heeney, M.; Anthopoulos, T. D.; de Mello, J.; McCulloch, I. *Macromolecules* **2011**, *44*, 6649.
(15) Piliego, C.; Holcombe, T. W.; Douglas, J. D.; Woo, C. H.; Beaujuge, P. M.; Fréchet, J. M. J. *J. Am. Chem. Soc.* **2010**, *132*, 7595.
(16) Yiu, A. T.; Beaujuge, P. M.; Lee, O. P.; Woo, C. H.; Toney, M. F.; Fréchet, J. M. J. *J. Am. Chem. Soc.* **2012**, *134*, 2180.
(17) Biniek, L.; Fall, S.; Chochos, C. L.; Anokhin, D. V.; Ivanov, D. A.; Leclerc, N.; Leveque, P.; Heiser, T. *Macromolecules* **2010**, *43*, 9779.
(18) Zhang, F.; Hu, Y.; Schuettfort, T.; Di, C.; Gao, X.; McNeill, C. R.; Thomsen, L.; Mannsfeld, S. C. B.; Yuan, W.; Sirringhaus, H.; Zhu, D. *J. Am. Chem. Soc.* **2013**, *135*, 2338.
(19) Lei, T.; Dou, J. H.; Pei, J. *Adv. Mater.* **2012**, *24*, 6457.
(20) Bronstein, H.; Chen, Z.; Ashraf, R. S.; Zhang, W.; Du, J.; Durrant, J. R.; Tuladhar, P. S.; Song, K.; Watkins, S. E.; Geerts, Y.; Wienk, M. M.; Janssen, R. A. J.; Anthopoulos, T. D.; Sirringhaus, H.; Heeney, M.; McCulloch, I. *J. Am. Chem. Soc.* **2011**, *133*, 3272.
(21) Zhang, X.; Richter, L. J.; DeLongchamp, D. M.; Kline, R. J.; Hammond, M. R.; McCulloch, I.; Heeney, M.; Ashraf, R. S.; Smith, J. N.; Anthopoulos, T. D.; Schroeder, B.; Geerts, Y. H.; Fischer, D. A.; Toney, M. F. *J. Am. Chem. Soc.* **2011**, *133*, 15073.